Volume 1 | Number 1 | Jan 2013 | Pages 1–100

Nanoscale

www.rsc.org/nanoscale

ROYAL SOCIETY
OF CHEMISTRY

ROYAL SOCIETY
OF CHEMISTRY

Non-exponential resistive switching in Ag$_2$S memristors: a key to nanometer-scale non-volatile memory devices

Agnes Gubicza,[*] **Miklós Csontos, András Halbritter and György Mihály**

The dynamics of resistive switchings in nanometer-scale metallic junctions formed between an inert metallic tip and an Ag film covered by a thin Ag$_2$S layer are investigated. Our thorough experimental analysis and numerical simulations revealed that the resistance change upon a switching bias voltage pulse exhibits a strongly non-exponential behaviour yielding to markedly different response times at different bias levels. Our results demonstrate the merits of Ag$_2$S nanojunctions as nanometer-scale non-volatile memory cells with stable switching ratios, high endurance as well as fast response to write/erase, and an outstanding stability against read operations at technologically optimal bias and current levels.

Future technological developments in non-volatile resistance switching random access memory (ReRAM) applications[1–3] exceeding the limitations of nowadays Flash devices[4] are expected to comply with the basic requirements of a small size for a high data storage density as well as fast read and write operations performed at reasonably low voltage and easily detectable current levels. Further important criteria involve high endurance against several writing cycles and a long retention time[5] which greatly rely on the long-term mechanical and electrical stability of the corresponding ON and OFF states. Moreover, it is also a key issue that such passive circuit elements exhibit a strongly non-linear response function, so that the device is stable against low-level read-out signals and, at the same time, it responds quickly to write operations carried out at higher biases.

Tunable, nanometer scale junctions formed between metallic electrodes by reversible solid state electrochemical reactions represent extremely promising candidates to satisfy the above criteria.[1,6–17] The resistive state of such a memory element, called memristor,[18] is altered by biasing the device above its writing threshold (V_{th}). Readout is performed at lower signal levels which preserve the stored information.

Previous studies on the dynamical properties of memristive systems[6,9,17,19–34] mostly focused on the formation and com-plete rupture of metallic filaments in solid state ionic conductors giving rise to extremely high R_{OFF}/R_{ON} ratios at practically insulating R_{OFF} and $R_{ON} \approx h/2e^2 = 12.9$ kΩ resistance values, the latter corresponding to atomic sized contacts. While the near-equilibrium conditions of low ionic and tunneling currents facilitated the identification of the underlying microscopic mechanisms in this regime, fundamental RC limitations only allowed the exploration of narrower segments in the time domain.

Our previous experiments[35] have shown that suitably prepared, nanometer scale junctions utilizing a 30 nm thick layer of the ionic conductor Ag$_2$S sandwiched between Ag and PtIr electrodes are capable of reproducible, nanosecond timescale switching operation at room temperature exhibiting R_{OFF}/R_{ON} ratios of $2-10$. Resistive switching takes place via metallic channels of diameters changing in the range of 2-5 nm which are subject to electric fields of the order of 10^6 V/cm and current densities of 10^{10} A/cm^2. The technologically optimal, metallic ON and OFF state resistance values of about 1 kΩ are fully compatible with nowadays CMOS standards. Moreover, the considerably lower writing (read-out) voltages of a few 100 mV (10 mV) applied for two orders of magnitude shorter times offer a significantly decreased power consumption.

Here we discuss the dynamics of the resistance change during such resistive switchings, representing a so far relatively unexplored area in memristor research. We demonstrate stable switching ratios over $>10^4$ writing cycles and the stability of the stored information. We show that the switchings can simultaneously exhibit fast and slow variations over more than eight orders of magnitude in time with characteristic time scales highly depending on the biasing conditions. This enables the utilization of Ag$_2$S based nanojunctions in non-volatile memory applications. The transition between two different states is found to be non-exponential in time reminiscent to the variation of the synaptic potential[36–38] also responsible for the short and long-term memory of the human brain.[20,39] The latter behaviour has been successfully accounted for by numerical simulations based on an empirical master equation.

Department of Physics, Budapest University of Technology and Economics and MTA-BME Condensed Matter Research Group, Budafoki ut 8, 1111 Budapest, Hungary. E-mail: gubicza@dept.phy.bme.hu

Nanoscale Accepted Manuscript

During sample fabrication a 80 nm thick Ag layer was deposited onto a Si substrate followed by a 5 minutes long sulfurisation. The S diffused into the Ag layer forming an approximately 30 nm thick Ag_2S layer on top of the Ag.[40] Nanometer scale junctions were created by gently touching the Ag_2S surface with a mechanically sharpened PtIr tip in an STM geometry. The V_{drive} voltage output of a low output impedance (5 Ω) arbitrary waveform generator was acting on the memristive junction and on the serial resistor R_s while the V_{bias} voltage drop on the junction was monitored by an oscilloscope as shown in the left inset of Fig. 1(a). By convention, a positive bias corresponds to positive voltage applied to the Ag layer with respect to the PtIr electrode. All measurements were performed at room temperature.

A typical current-voltage (I-V) trace recorded within 1 ms is illustrated in the right inset of Fig. 1(a). At low bias voltages the initial OFF state resistance R_{OFF} is measured. Increasing V_{bias} to V_{th} = 200 mV a reconfiguration takes place resulting in a drop of the junction's resistance from R_{OFF} = 70 Ω to R_{ON} = 38 Ω. Lowering V_{bias} preserves the R_{ON} ON state resistance until a negative threshold of -300 mV is reached where the initial OFF state is restored. The direction of the resulting hysteresis loop is indicated by the arrows in the inset.

Resistive switchings can also be initiated by voltage pulses as demonstrated in Fig. 1(a) and Fig. 1(b) for different pulse durations in two representative junctions. In each case the junction is prepared in its higher resistance OFF state by a high amplitude negative voltage pulse of V_{drive} =-1.3 V [Fig. 1(a)] and -4.5 V [Fig. 1(b)] (not shown). R_{OFF} is measured at a low positive read-out voltage. This is followed by a high amplitude positive pulse (V_{drive} =+1.3 V and +4.5 V, respectively) to switch the device to its lower resistance ON state. Again, a low read-out voltage is applied to determine R_{ON} in the final state. Note that due to $R_s > R_{OFF}$ the observed change is more dominant in the voltage response of each device compared to its current variation. While Fig. 1(a) demonstrates that the junction exhibits a significant resistance change even at the time scale of the 1 ms long switching pulse, a three orders of magnitude faster operation is exemplified in Fig. 1(b) where a resistance change by a factor of ≈2 is achieved within 500 ns. Moreover, our previous experiments showed that resistive switchings can be initiated by voltage pulses as short as 500 ps.[35] These observations indicate that fast and slow switching processes can co-exist in Ag_2S based nanojunctions. In the main part of this paper we exploit this unique behaviour by a thorough analysis of the switching characteristics under various biasing conditions.

The colour map of Fig. 2(a) displays the R_{OFF}/R_{ON} ratio deduced from the zero-bias slopes of the $> 10^4$ individual I-V traces acquired on a representative, stable device at different f_{drive} frequencies and V_{drive}^0 amplitudes of the driving triangle signal and using R_s = 51 Ω. By gradually increas-
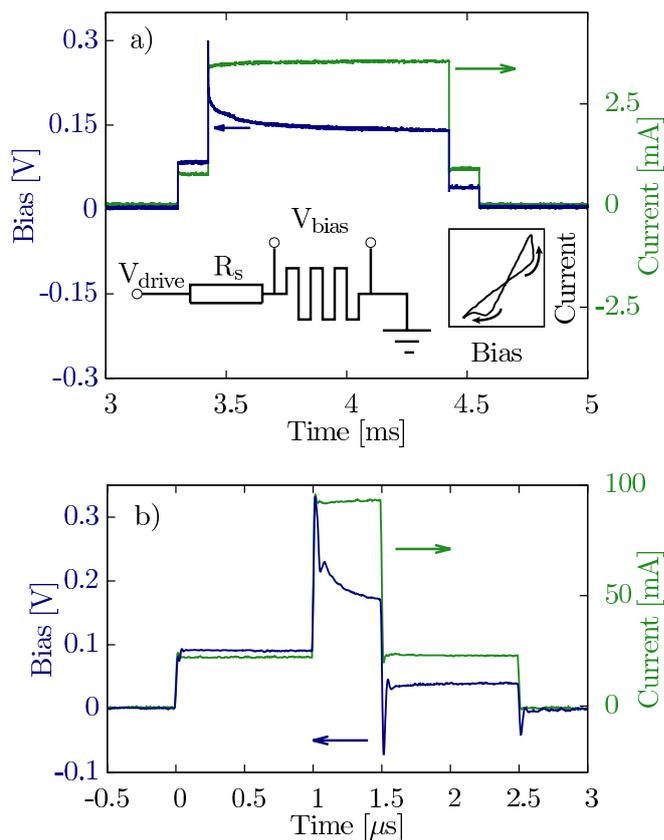

Fig. 1 Resistive switching initiated by 1 ms a) and 500 ns b) long voltage pulses. The positive bias corresponds to positive voltage applied to the Ag layer with respect to the PtIr tip. The blue curves represent the voltage drop on the junction. The green traces correspond to the current flowing through the device. The insets show a typical I-V characteristics acquired within 1 ms as well as the electrical circuit diagram of the biasing setup. The 1 ms long voltage pulse was applied with R_s = 330 Ω on a junction exhibiting R_{OFF} = 110 Ω and R_{ON} = 41 Ω. During the 500 ns pulse R_s = 50 Ω was used in series with R_{OFF} = 5 Ω and R_{ON} = 2 Ω.

ing V_{drive}^0 above a switching threshold the R_{OFF}/R_{ON} ratio exceeds unity. We have repeatedly increased V_{drive}^0 at various driving frequencies until R_{OFF}/R_{ON} = 4 was achieved. The data shows a clear logarithmical increase in the switching threshold towards higher frequencies. The regions of constant $\alpha = R_{OFF}/R_{ON}$ ratios can be well approximated by the formula

$$V_{drive} = a \cdot lg(f_{drive}) + b, \tag{1}$$

where the parameters a, b and α are characteristic to a specific junction and its observed switching, while $T = 1/f_{drive}$ is the characteristic time scale of the resistance change. This tendency holds over 6 orders of magnitude in the frequency domain and is further illustrated by the two sets of selected
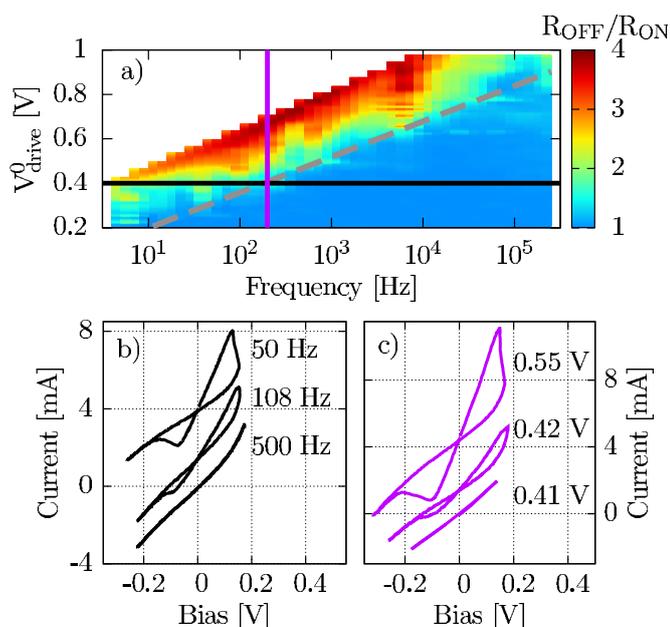
Fig. 2 a) Resistance ratio $\alpha = R_{OFF}/R_{ON}$ as a function of the driving frequency and amplitude. The dashed line is a guide to the eye visualizing the empirical relation of Eq. 1 describing the $\alpha = $ constant regions. b) Selected I-V traces taken at $V_{drive}^0 = 0.4$ V and various frequencies along the black line indicated in a). c) I-V traces taken at $f_{drive} = 200$ Hz with different amplitudes along the magenta line in a). The curves in b) and c) are vertically shifted for clarity.

I-V traces shown in Fig. 2(b) and Fig. 2(c) corresponding to the constant amplitude and constant frequency cuts of the data shown in Fig. 2(a) along the black and magenta solid lines, respectively. At $V_{drive}^0 = 0.4$ V resistive switching can only be observed below driving frequencies of $f_{drive} \approx 100$ Hz, while at $f_{drive} = 200$ Hz the onset of the resistive switching takes place above $V_{drive}^0 = 0.42$ V.

Our data reveals that in spite of the statistical nature of the microscopic processes responsible for the observed resistive switching, the R_{OFF}/R_{ON} ratio is a monotonous function of the driving amplitude and one needs larger V_{drive}^0 to initiate faster resistance changes while at a certain frequency a well established threshold voltage sets in. Note that increasing V_{drive}^0 results in a larger resistance change while the maximal V_{bias} voltage drop on the memristive element is locked to the threshold voltage at increasing device currents (quasi-vertical part of the I-V curve). We found that different junctions exhibit a qualitatively similar logarithmic relation between the threshold amplitude and the frequency, however, the actual parameters of this relation may moderately vary from device to device.

In order to gain a more detailed insight into the dynamics of the resistive switchings we monitored the R(t) resistance of
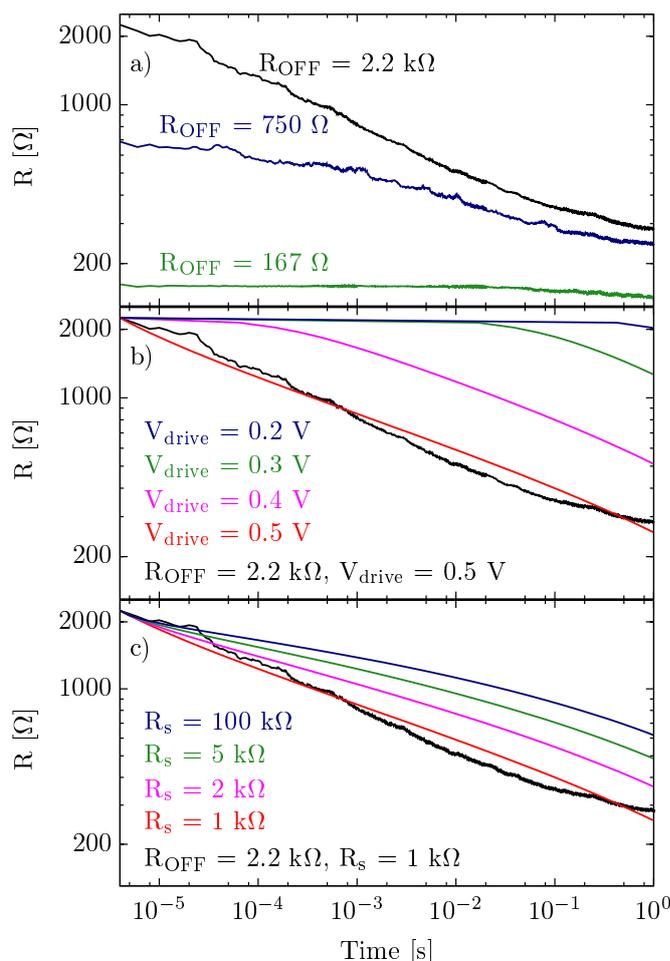

Fig. 3 a) Junction resistances R(t) recorded during 1 s long rectangular voltage pulses of different amplitudes at various R_{OFF} initial resistances. $R_s = 1$ kΩ, $V_{drive} = 0.5$ V (black), $R_s = 1330$ Ω, $V_{drive} = 1$ V (blue), $R_s = 1330$ Ω, $V_{drive} = 0.9$ V (green). b) The results of numerical simulations for R(t) at varying V_{drive} at $R_{OFF} = 2.2$ kΩ and $R_s = 1$ kΩ. c) Similar simulations performed at varying R_s and V_{drive} at identical initial $V_{bias}(0) = 0.35$ V and $R_{OFF} = 2.2$ kΩ. The black lines in b) and c) represent the data shown in a) with $R_{OFF} = 2.2$ kΩ, $R_s = 1$ kΩ and $V_{drive} = 0.5$ V.

the junction over six decades in the time domain with a resolution of 2 μs during a 1 s positive rectangular voltage pulse for various V_{drive} amplitudes, R_s series resistors and R_{OFF} initial resistances. Fig. 3(a) shows three representative experimental R(t) traces on a log-log scale. The black curve corresponding to a junction with $R_{OFF} = 2.2$ kΩ shows a gradual variation over more than 5 orders of magnitude in time, whereas the resistance corresponding to $R_{OFF} = 167$ Ω (green curve) only changes during the last one and a half decade. It is to be emphasized that none of the three curves can be properly described by introducing a single time constant. While, for

instance, an exponential fit to the initial part of the black trace provides a time constant of 10 μs, R(t) around the falling edge of the V_{drive} pulse can be the best described by a time constant of 10 s. Consistently with the tendency shown in Fig. 2, this markedly different behaviour is attributed to the different $V_{bias}(0) = V_{drive}R_{OFF}/(R_s + R_{OFF})$ initial voltage drop acting on the device, *i.e.*, shorter characteristic time scales can be achieved at higher $V_{bias}(0)$ values. As R(t) is decreasing toward the final R_{ON} resistance, $V_{bias}(t)$ also undergoes a downscaling in the fashion of the above formula, resulting in a further slowdown of the resistance change which becomes observable even up to seconds. We point out that the former issue, *i.e.*, the fast (slow) resistance change at high (low) V_{bias} is inevitable for fast write/erase (slower, non-volatile read-out) operations in ReRAM applications. The gradual transition behavior from the OFF to the ON state under a constant voltage application is markedly different from the sharp transition observed in atomic switches.[41] This is attributed to the role of multiple degrees of freedom in our system consisting of metallic channels of 2-5 nm in diameter[35] instead of single atoms in the narrowest cross-section of the junction. We speculate that the dominating driving force of the resistance change is still electric field driven activated ionic transport giving rise to the expansion/shrinkage of the metallic conduction channel which is determined by its local asymmetry around the narrowest cross-section of the junction. However, the considerable self-heating of the junction and the electron wind forces due to high current densities may also play role in the resistive switching. Identifying the detailed microscopical mechanisms is a subject of ongoing molecular dynamical simulations.

The observed behaviour was also accounted for by a time-dependent numerical simulation demonstrating that due to their common origin the time dependence of the resistance change during a voltage pulse [Fig. 3(a)] is necessarily consistent with the bias and frequency dependence of the switching ratios, as determined from complete I-V traces (Fig. 2). Based on the empirical logarithmic relation deduced from the data shown in Fig. 2(a) we assume that a resistance change of $\alpha = R(t)/R(t+\Delta t)$ takes place within a characteristic time of $\Delta t = 10^{-[V_{bias}-b]/a}$ in the fashion of Eq. 1, where $V_{bias} = V_{drive} \cdot R(t)/(R(t)+R_s)$ is the actual voltage drop acting on the junction. During the numerical implementation the initial resistance value R(1) was chosen to be equal to R_{OFF} at the time t(1) = 0. The $\Delta t(n+1)$ time required to achieve the next resistance value $R(n+1) = R(n)/\alpha$ was determined by the above formulae in each iteration step.

The results of the simulations performed at various V_{drive} and constant R_{OFF} and R_s as well as at various R_s but identical $V_{bias}(0)$ values and constant R_{OFF} are illustrated in Figs. 3(b) and 3(c), respectively. The black experimental trace of Fig. 3(a) characterized by the same parameters as the red simulated line is re-plotted in Figs. 3(b) and 3(c) for com-
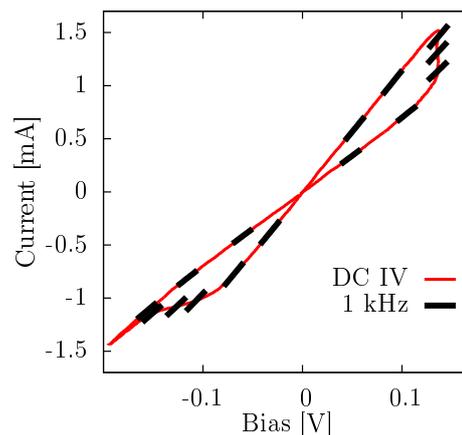

Fig. 4 I-V trace recorded at a slow bias signal of f = 1 Hz (red). The results of a simultaneous lock-in measurement performed at an AC modulation of f = 1 kHz along the DC curve are represented by the black dashes.

parison. It is evident that simulation not only describes the selected experimental time traces by using exclusively predetermined empirical values but the two sets of curves also properly account for the observed tendencies attributed to the complementary effects of changing $V_{bias}(0)$ and R_{OFF}/R_s. Note that the parameters *a*, *b* and α used to construct the traces of Figs. 3(b) and 3(c) correspond to a different junction and are therefore different from the ones describing the data shown in Fig. 2(a) within a factor of two.

The above described emergence of the different time scales during the switching process can be further visualized by mixing a small amplitude, high frequency modulation to a slowly varying, higher amplitude triangle driving signal and utilize lock-in detection to determine the finite bias current-to-voltage response of the junction. This technique enables the separation of the characteristic time scales governing the resistance change of the junction. If the change is fast enough to follow the AC modulation, the lock-in detected signal is expected to return the dI/dV_{bias} derivative of the I-V curve. On the contrary, if the lock-in frequency exceeds the speed of the internal processes in the system, the junction is unable to change its resistance during one period of the lock-in excitation. Hence the latter is not expected to detect the differential resistance but only the actual Ohmic resistance of the junction.

Figure 4 shows the result of the simultaneous AC&DC detection of a typical I-V trace. Both the AC and DC components were applied over $R_s \gg R_{OFF}$ serial resistors adding a $V_{bias}^{ac} \approx$ 1 mV, *f* = 1 kHz modulation to the DC trace recorded within 1 s. The red line in Fig. 4 displays a DC I-V trace while the slopes of the black dashes shown at selected finite bias values represent the harmonic response measured by the lock-in amplifier. Whereas in the well defined ON and OFF states both
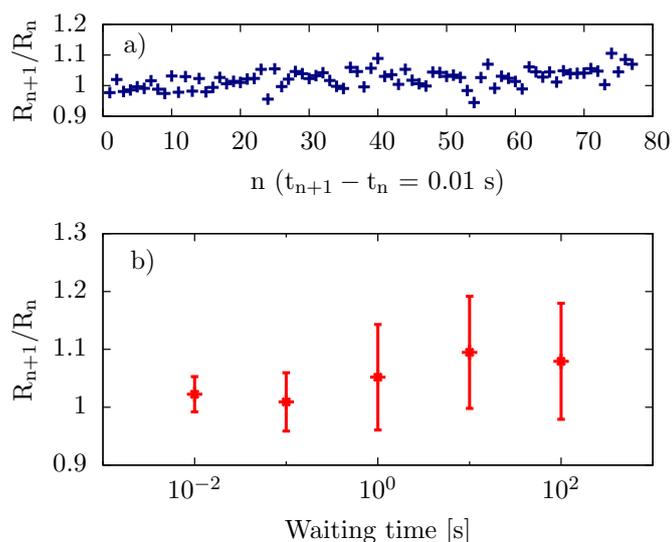
Fig. 5 Analysis of the system stability during the waiting time Δt between two subsequent I-V measurements. a) The ratio of the $(n+1)^{th}$ and n^{th} resistances R_{n+1}/R_n at $V_{drive} = 0$ V applied during $\Delta t = 0.01$ s. b) The average and standard deviation of R_{n+1}/R_n as a function of Δt.

the AC and DC methods accurately return the actual dI/dV_{bias} values, it is evident that under these conditions the internal time-scale of the system was too long to follow the AC modulation during the resistive switchings, giving rise to a harmonic response corresponding to the Ohmic resistance of the junction. It is to be added that a qualitatively similar behaviour was found in various junctions tested in the 1 kHz$< f <$100 kHz lock-in frequency domain, in agreement with the quantitative predictions deduced from Fig. 2.

The data presented in Fig. 2 and Fig. 3 clearly indicate that the R_{OFF}/R_{ON} ratio not only depends on the driving amplitude but also on the time-scale of the applied biases thus making a universal switching threshold ill-defined. This raises the question whether a non-volatile memory element built on the Ag_2S ionic conductor platform can preserve (i) its ON and OFF state resistances during repeated write/erase cycles and (ii) the stored information against the voltage noise arising from the environment in its unbiased state.

Figure 5 demonstrates the long-term stability of our system. We measured subsequent I-V curves of the same junction separated by different waiting times while zero bias voltage was applied to the device, thus extending our investigations by further two orders of magnitude in the time domain. Figure 5(a) shows the ratio of the initial OFF state resistance evaluated from the corresponding zero-bias slope of the $(n+1)^{th}$ trace and the final, also OFF state resistance of the previous, n^{th} loop. The waiting time was set to 0.01 s during which the junction was left unbiased. The obtained variation of the above

defined resistance ratio is less than 5% over 100 measurement cycles performed within a second. Such a variation is negligible compared to the $R_{OFF}/R_{ON} \approx 4$ switching ratio deduced from the individual I-V traces representing an excellent electronic and mechanical stability. This measurement scheme was repeated with various waiting times ranging from 0.01 s to 100 s. The average and standard deviation of R_{n+1}/R_n is plotted against the waiting time in Fig. 5(b) showing an average ratio close to 1 even at 100 s waiting times where the mechanical stability of our zero feedback STM setup becomes a concern.

In conclusion, we studied the dynamics of the resistive switchings in Ag-Ag_2S-PtIr nanojunctions. We showed that the resistance change simultaneously exhibits multiple time scales ranging from a nanosecond to seconds upon a switching voltage pulse. The resulting non-exponential transition between the OFF and ON states as well as the achievable, technologically convenient $R_{OFF}/R_{ON} = 2 - 10$ ratios are largely affected by the amplitude and frequency of the biasing signals. This fundamental, inherent property of the Ag_2S ionic conductor provides the unique opportunity for the combination of GHz write/erase operations performed at bias levels of a few Volts, non-volatile read-out with slower signals of a few 10 mV and robust information storage at zero bias in a two terminal, nanometer scale analog memory device. Additionally, the observed non-exponential behaviour along with the access to tunable multiple resistance states[41] open a wide range of novel applications including integrated processing and storage platforms[42], multiple bit based computation schemes[43] and improved neural network modeling.[44–46]

References

1 J. J. Yang, D. B. Strukov and D. R. Stewart, *Nat. Nano*, 2013, **8**, 13–24.
2 J. Borghetti, G. S. Snider, P. J. Kuekes, J. J. Yang, D. R. Stewart and R. S. Williams, *Nature*, 2010, **464**, 873–876.
3 Y. V. Pershin and M. Di Ventra, *Phys. Rev. E*, 2011, **84**, 046703.
4 A. Chung, J. Deen, J.-S. Lee and M. Meyyappan, *Nanotechnology*, 2010, **21**, 412001.
5 R. Waser, R. Dittmann, G. Staikov and K. Szot, *Adv. Mater.*, 2009, **21**, 2632–2663.
6 K. Terabe, T. Hasegawa, T. Nakayama and M. Aono, *Nature*, 2005, **433**, 47–50.
7 D. B. Strukov, G. S. Snider, D. R. Stewart and R. S. Williams, *Nature*, 2008, **453**, 80–83.
8 R. Waser and M. Aono, *Nat. Mater.*, 2007, **6**, 833–840.
9 K. Terabe, T. Hasegawa, C. Liang and M. Aono, *Adv. Mater.*, 2007, **8**, 536–542.
10 Z. Wang, T. Kadohira, T. Tada and S. Watanabe, *Nano Lett.*, 2007, **7**, 2688–2692.
11 S. H. Jo and W. Lu, *Nano Lett.*, 2008, **8**, 392–397.

Nanoscale Accepted Manuscript

12 M. Aono and T. Hasegawa, *IEEE Proc.*, 2010, **898**, 2228–2236.

13 E. Linn, R. Rosezin, C. Kugeler and R. Waser, *Nat. Mater.*, 2010, **9**, 403–406.

14 Y. V. Pershin and M. Di Ventra, *Adv. Phys.*, 2011, **60**, 145–227.

15 I. Valov, R. Waser, J. R. Jameson and M. N. Kozicki, *Nanotechnology*, 2011, **22**, 254003.

16 A. C. Torrezan, J. P. Strachan, G. Medeiros-Ribeiro and R. S. Williams, *Nanotechnology*, 2011, **22**, 485203.

17 T. Hasegawa, K. Terabe, T. Tsuruoka and M. Aono, *Adv. Mater.*, 2012, **24**, 252–267.

18 L. Chua, *IEEE Trans. Circuit Theory*, 1971, **18**, 507 – 519.

19 T. Chang, S.-H. Jo and W. Lu, *ACS Nano*, 2011, **5**, 7669–7676.

20 T. Ohno, T. Hasegawa, T. Tsuruoka, K. Terabe, J. K. Gimzewski and M. Aono, *Nat. Mater.*, 2011, **10**, 591–595.

21 J. J. T. Wagenaar, M. Morales-Masis and J. M. van Ruitenbeek, *J. Appl. Phys.*, 2012, **111**, 014302.

22 D. B. Strukov and R. S. Williams, *Appl. Phys. A*, 2008, **94**, 515–519.

23 Z. Xu, Y. Bando, W. Wang, X. Bai and D. Golberg, *ACS Nano*, 2010, **4**, 2515–2522.

24 A. Nayak, T. Tamura, T. Tsuruoka, K. Terabe, S. Hosaka, T. Hasegawa and M. Aono, *J. Phys. Chem. Lett.*, 2010, **1**, 604–608.

25 M. Morales-Masis, S. J. van der Molen, W. T. Fu, M. B. Hesselberth and J. M. van Ruitenbeek, *Nanotechnology*, 2009, **20**, 095710.

26 M. Morales-Masis, H.-D. Wiemhöfer and J. M. van Ruitenbeek, *Nanoscale*, 2010, **2**, 2275–2280.

27 M. Morales-Masis, S. J. van der Molen, T. Hasegawa and J. M. van Ruitenbeek, *Phys. Rev. B*, 2011, **84**, 115310.

28 A. Nayak, T. Tsuruoka, K. Terabe, T. Hasegawa and M. Aono, *Appl. Phys. Lett.*, 2011, **98**, 233501.

29 S. Menzel, U. Böttger and R. Waser, *J. Appl. Phys.*, 2012, **111**, 014501.

30 I. Valov, I. Sapezanskaia, A. Nayak, T. Tsuruoka, T. Bredow, T. Hasegawa, G. Staikov, M. Aono and R. Waser, *Nat. Mater.*, 2012, **11**, 530–535.

31 Y. Yang, P. Gao, S. Gaba, T. Chang, X. Pan and W. Lu, *Nat. Comm.*, 2012, **3**, 732.

32 Q. Liu, J. Sun, H. Lv, S. Long, K. Yin, N. Wan, Y. Li, L. Sun and M. Liu, *Adv. Mater.*, 2012, **24**, 1844–1849.

33 S. Menzel, S. Tappertzhofen, R. Waser and I. Valov, *Phys. Chem. Chem. Phys.*, 2013, **15**, 6945–6952.

34 Y. Yang and W. Lu, *Nanoscale*, 2013, **5**, 10076–10092.

35 A. Geresdi, M. Csontos, A. Gubicza, A. Halbritter and G. Mihály, *Nanoscale*, 2014, **6**, 2613.

36 D. C. Rubin, S. Hinton and A. Wenzel, *Journal of Experimental Psychology: Learning, Memory and Cognition*, 1999, **25**, 1161–1176.

37 S. H. Jo, T. Chang, I. Ebong, B. B. Bhadviya, P. Mazumder and W. Lu, *Nano Letters*, 2010, **10**, 1297–1301.

38 D. Kuzum, R. G. D. Jeyasingh, B. Lee and H.-S. P. Wong, *Nano Letters*, 2012, **12**, 2179–2186.

39 R. Yang, K. Terabe, Y. Yao, T. Tsuruoka, T. Hasegawa, J. K. Gimzewski and M. Aono, *Nanotechnology*, 2013, **24**, 384003.

40 A. Geresdi, A. Halbritter, E. Szilágyi and G. Mihály, *MRS Proceedings*, 2011, vol. 1331.

41 C. Schirm, M. Matt, F. Pauly, J. C. Cuevas, P. Nielaba and E. Scheer, *Nat. Nano*, 2013, **8**, 645.

42 M. Di Ventra and Y. V. Pershin, *Nature Physics*, 2013, **9**, 200–202.

43 X. Zhao and H. Long, *IEEE Evolutionary Computation*, 2005, **3**, 1996–2001.

44 K. K. Likharev, *Science of Advanced Materials*, 2011, **3**, 322–331.

45 D. Kuzum, S. Yu and H.-S. P. Wong, *Nanotechnology*, 2013, **24**, 382001.

46 A. Thomas, *Journal of Physics D: Applied Physics*, 2013, **46**, 093001.

Nanoscale Accepted Manuscript